

Thermal conductivity and ballistic-phonon transport in the cross-plane direction of superlattices

G. Chen

Mechanical and Aerospace Engineering Department, University of California, Los Angeles, California 90095

(Received 24 July 1997; revised manuscript received 19 February 1998)

Significant reductions in both the in-plane and cross-plane thermal conductivities of superlattices, in comparison to the values calculated from the Fourier heat conduction theory using bulk material properties, have been observed experimentally in recent years. Understanding the mechanisms controlling the thermal conductivities of superlattice structures is of considerable current interest for microelectronic and thermoelectric applications. In this work, models of the thermal conductivity and phonon transport in the direction perpendicular to the film plane of superlattices are established based on solving the phonon Boltzmann transport equation (BTE). Different phonon interface scattering mechanisms are considered, including elastic vs inelastic, and diffuse vs specular scattering of phonons. Numerical solution of the BTE yields the effective temperature distribution, thermal conductivity, and thermal boundary resistance (TBR) of the superlattices. The modeling results show that the effective thermal conductivity of superlattices in the perpendicular direction is generally controlled by phonon transport within each layer and the TBR between different layers. The TBR is no longer an intrinsic property of the interface, but depends on the layer thickness as well as the phonon mean free path. In the thin layer limit, phonon transport within each layer is ballistic, and the TBR dominates the effective thermal conductivity of superlattices. Approximate analytical solutions of the BTE are obtained for this thin-film limit. The modeling results based on partially specular and partially diffuse interface scattering processes are in reasonable agreement with recent experimental data on GaAs/AlAs and Si/Ge superlattices. From the modeling, it is concluded that the cross-plane thermal conductivity of these superlattices is controlled by diffuse and inelastic scattering processes at interfaces. Results of this work suggest that it is possible to make superlattice structures with thermal conductivity totally different from those of their constituting materials. [S0163-1829(98)04523-8]

I. INTRODUCTION

Thermal conductivities of superlattice structures are attracting increasing attention due to their importance in different applications such as the development of thermoelectric devices and the thermal management of semiconductor lasers. Studies over the past few years have demonstrated that the thermoelectric effects in quantum-well structures can be greatly enhanced above their corresponding bulk materials.^{1,2} To realize highly efficient thermoelectric devices, the thermal conductivity of superlattice structures should be minimized. Conversely, for semiconductor lasers, the thermal conductivity of quantum wells and the surrounding structures, particularly the Bragg reflectors in vertical-cavity surface-emitting lasers, should be maximized.³ These applications have inspired several experimental studies on the thermal conductivity of superlattice structures. Yao⁴ performed the first measurement on the thermal conductivity of GaAs/AlAs superlattice structures in the in-plane direction. His experiment showed that the thermal conductivities of the measured superlattices with equal layer thickness are smaller than that of these structures calculated according to the Fourier heat conduction theory based on the thermal conductivities of bulk GaAs and AlAs, but larger than that of Ga_{0.5}Al_{0.5}As alloy. Chen *et al.*⁵ measured the thermal conductivity of a GaAs/Al_xGa_{1-x}As multilayer structure for vertical-cavity surface-emitting lasers in both the in-plane and cross-plane directions. Their results indicate that the thermal conductivity of GaAs/Al_xGa_{1-x}As in the cross-plane direction can be smaller than their corresponding alloy. This phenomenon is more clearly demonstrated in the experiment

of Capinski and Maris⁵ on the temperature dependence of the thermal conductivity of two GaAs/AlAs superlattices in the cross-plane direction. The temperature dependence of the in-plane thermal conductivity of a thick-period GaAs/AlAs superlattice was reported by Yu *et al.*⁶ More recently, Lee, Cahill, and Venkatasubramanian⁷ measured thermal conductivities of several Si/Ge superlattices in the cross-plane direction, and further demonstrated that the thermal conductivities of superlattices in this direction can be smaller than those of their corresponding alloys. Similar results have been obtained on Bi₂Te₃/Sb₂Te₃ superlattices.⁸ In addition to semiconductor superlattices, experimental results on the thermal conductivities of other types of periodic thin-film structures have also been reported.^{9,10}

The thermal conductivity of superlattices may differ from the prediction of the Fourier heat conduction theory based on bulk material properties due to the presence of interfaces. The new periodicity in a superlattice structure can alter the lattice vibrational properties, i.e., the phonon spectra, of its constituent materials.¹¹⁻¹³ The change in phonon spectra results from the interference effects among phonon waves scattered at the interfaces, in analogy to the electron interference and transport in superlattice structures.¹⁴ Narayanamurti *et al.*¹¹ first observed phonon interference effects in superlattices by measuring phonon transmission through superlattices at low temperatures. Many subsequent studies on the phonon spectra of superlattices further confirmed the formation of minibandgaps in superlattices due to phonon interference.^{12,13} This interference effect is best observed at low temperatures when the dominant phonon wavelength is long. At room temperature, the dominant phonon wavelength

is $\sim 10 \text{ \AA}$ in GaAs.¹⁵ Phonon transport in films much thicker than 10 \AA can be described by treating phonons as particles, and is governed by the Boltzmann transport equation (BTE). The presence of the interfaces in superlattices, however, can affect the transport properties as long as the phonon mean free path (MFP) is comparable to or longer than the film thickness. This is the classical size effect transport regime. Studies of such a classical size effect on the electrical conductivity have been abundant.¹⁶ There have also been increasing research activities concerning size effects on the thermal conductivity of thin films, particularly during the last decade.¹⁷ The first study on the thermal conductivity of superlattices was carried out by Ren and Dow.¹⁸ They modeled the thermal conductivity of idealized Ge-type superlattice structures by combining the classical BTE approach¹⁹ with a quantum-mechanical treatment of the additional scattering process caused by the minibandgaps. The predicted reduction of the peak thermal conductivity from their model, however, is too small ($< 25\%$) to explain the experimentally observed 1–2 order-of-magnitude reduction of the thermal conductivity of semiconductor superlattices. Chen¹⁵ and Hyldgaard and Mahan,²⁰ established models based on the BTE to calculate the thermal conductivity of superlattice structures in the direction parallel to the film plane. Neither of these two studies includes the phonon interference effects. Results of these models, however, demonstrated reasonable agreement with the experimental data of Yao⁴ and Yu *et al.*⁶ on GaAs/AlAs superlattices in the same direction. These studies suggest that the BTE is applicable for superlattices and periodic structures with relatively thick constituent layers, and that diffuse interface scattering is the key factor in explaining the observed reduction in the thermal conductivity of GaAs/AlAs superlattices. Chen's study¹⁵ further shows that the in-plane thermal conductivity is very sensitive to the specularly of interface for phonon scattering. Totally specular phonon scattering at interfaces does not have much effect on the in-plane thermal conductivity of superlattice structures. A slight increase in the portion of diffuse phonon scattering, however, significantly reduces the superlattice thermal conductivity. His modeling results indicate the possibility of reducing the in-plane thermal conductivity of superlattices below that of their corresponding alloys, and suggest the possibility of engineering the superlattices to reduce their thermal conductivities without much penalty in the electronic transport properties.

Chen²¹ also modeled the phonon transport and the effective thermal conductivity of superlattice structures based on the BTE for heat flow across superlattice planes by assuming that phonons are scattered totally diffusely or totally specularly at the interface. The diffuse scattering model results were in reasonable agreement with experimental results of Capinski and Maris on a GaAs/AlAs superlattice.⁵ Hyldgaard and Mahan²² studied the thermal conductivity of a Si/Ge superlattice through the consideration of the phonon group velocity modification in superlattices by assuming totally specular interface scattering. Results from their model show that an order-of-magnitude reduction in the thermal conductivity of Si/Ge superlattices is possible due to the acoustic mismatch between Si and Ge. More recently, Chen and Neagu²³ considered both diffuse and specular, but inelastic, interface scattering of phonons at interfaces of super-

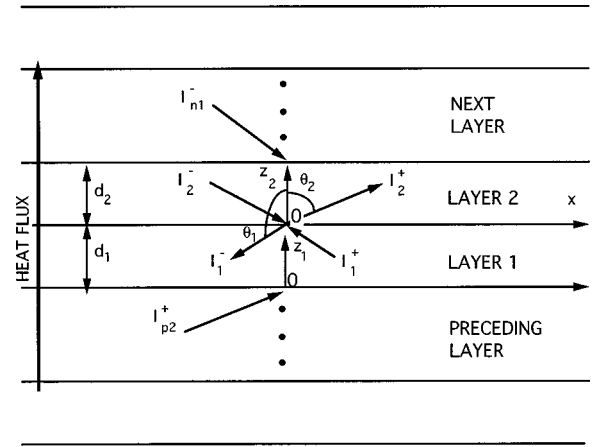


FIG. 1. Model and coordinate system.

lattices. Their modeling results point to the importance of diffuse interface scattering in explaining the experimental results on the cross-plane thermal conductivity of GaAs/AlAs and Si/Ge superlattices. These models, however, cannot deal with interfaces that scatter phonons partially diffusely and partially specularly, making it difficult to compare with the in-plane model¹⁵ that suggests a strong influence of the interface conditions on the superlattice thermal conductivity.

In this work, several models on the effective thermal conductivity of superlattices for heat flow in the direction perpendicular to the film plane are presented, based on solving the BTE for partially specular and partially diffuse interface scattering of phonons, with different interface scattering mechanisms. Section II describes these models and their underlying assumptions, followed by a discussion of the interface scattering processes, the thermal boundary resistance (TBR), and the mathematical treatment of the governing equations. Such a treatment leads to a set of integral equations describing the temperature gradient distribution within each layer, the phonon intensity distribution, and the TBR at the interfaces. Approximate analytical solutions of these equations, based on the observation of the numerical solution that the majority of the temperature drop across one period of a superlattice occurs at the interfaces, are also presented in this section. Section III discusses the numerical solution of the governing equations, and compares the solution with approximate analytical solutions and experimental results. These results show that the effective thermal conductivity of superlattice structures is generally controlled by heat transfer within each layer and the TBR between different layers, and that the TBR is no longer an intrinsic property of the interface but depends on the layer thickness and the phonon MFP. In the very thin-film limit, however, the effective thermal conductivity is dominated by the interface TBR.

II. THEORETICAL MODELS AND ANALYSIS

The focus of this work is on the phonon transport when the heat-flow direction is perpendicular to the superlattice film plane, as shown in Fig. 1, although it is believed that some of the results obtained in this work can be extended to heat transfer by photons in periodic structures. Phonon transport in this type of structures possesses the following three characteristics. First, the wave nature of phonons may be

come important, as indicated in the phonon spectra of superlattices.¹³ Second, as the constituent layers become thicker than the phonon coherence length,¹⁵ wave effects gradually disappear but the phonon MFP can be still larger than the layer thickness. Unlike a single layer with free surface types of boundary conditions, phonons in one layer can transmit through the interfaces ballistically, and thus affect the temperature distributions in other layers directly. Third, the interface will create additional resistance to the heat flow. To establish a model for heat conduction in a multilayer thin-film structure, the following two approximations are made: (1) films are thick enough such that the phonon spectrum in each layer can be represented by that of its bulk material, and (2) the spectral-dependent scattering rate in the bulk medium is approximated by an average MFP. The first approximation excludes phonon wave effects, and the second one is a gray-medium approximation. The validity and limitations of these two approximations have been discussed in detail in a previous paper on the thermal conductivity of superlattices in the in-plane direction.¹⁵ More discussion pertinent to transport in the cross-plane direction will be given in Sec. III.

Under the above-stated approximations, the BTE is applicable to phonon transport across superlattices, and can be expressed in terms of the total phonon intensity defined as,^{24,25}

$$I_i = \frac{1}{4\pi} \sum_m \int_0^{v_{\max}} |v_{mi}| f h \nu D_{mi}(\nu) d\nu, \quad (1)$$

where the subscript i ($=1,2$) denotes properties of one of the two adjacent layers, D is the density of states per unit volume, f the phonon distribution function, h the Planck constant, $|v_{mi}|$ the magnitude of the phonon group velocity, and ν the phonon frequency. The summation index m is over the three phonon polarizations.

The BTE, under the single-mode relaxation-time approximation, can be written as^{24,25}

$$\sin \theta_i \cos \varphi_i \frac{\partial I_i}{\partial x} + \cos \theta_i \frac{\partial I_i}{\partial z_i} = -\frac{I_i - I_{oi}}{\Lambda_i}, \quad (2)$$

where I_{oi} is the equilibrium phonon intensity in the i th layer that is obtained by substituting f in Eq. (1) with the Bose-Einstein distribution, θ and φ are the polar and the azimuthal angles, respectively, and Λ the average phonon MFP that could be estimated from the thermal conductivity k , the volumetric specific heat C , and the phonon group velocity ν , of bulk materials from

$$k = C \nu \Lambda / 3. \quad (3)$$

We should point out that the purpose of introducing the phonon intensity concept is for the mathematical convenience, particularly because the concept of photon intensity is widely used in thermal radiation.²⁶ By introducing the phonon intensity, the BTE becomes similar to the radiative transfer equation, and many results in radiative transfer can be used for phonon transport studies.²⁴ Although intensity is a function of both location and direction, as is clear from Eq. (2), it is a scalar quantity. The directional dependence of intensity is due to the directional dependence of the distribu-

tion function, because Eq. (1) is a scalar transformation. The distribution function is a scalar in the six-dimensional phase space (three space coordinates and three wave-vector coordinates).²⁷ Its directional dependence is a result of expressing the velocity coordinates in the three-dimensional space coordinates.

For heat conduction perpendicular to the superlattice plane, the phonon distribution function does not depend on x . A formal solution of Eq. (2) can be obtained by introducing a deviation function i_i ,

$$i_i(z_i, \theta_i) = I_i(z_i, \theta_i) - I_{oi}(T_i), \quad (4)$$

to rewrite Eq. (2) as

$$\cos \theta_i \frac{\partial i_i}{\partial z_i} + \frac{i_i}{\Lambda_i} = -\cos \theta_i \frac{dI_{oi}}{dz}. \quad (5)$$

The solution of the above equation in terms of the equilibrium phonon intensity has been well documented,²⁶

$$\begin{aligned} i_i(\eta_i, \mu_i) &= i_i^+(\eta_i, \mu_i) = i_i^+(0, \mu_i) e^{-\eta_i/\mu_i} \\ &\quad - \int_0^{\eta_i} \frac{dI_{oi}}{dt_i} e^{-(\eta_i-t_i)/\mu_i} dt_i \\ &\quad (\text{for } 0 < \mu_i < 1) \end{aligned} \quad (6)$$

$$\begin{aligned} i_i(\eta_i, \mu_i) &= i_i^-(\eta_i, \mu_i) = i_i^-(\xi_i, \mu_i) e^{(\xi_i-\eta_i)/\mu_i} \\ &\quad + \int_{\eta_i}^{\xi_i} \frac{dI_{oi}}{dt_i} e^{-(\eta_i-t_i)/\mu_i} dt_i \\ &\quad (\text{for } -1 < \mu_i < 0) \end{aligned} \quad (7)$$

where μ_i ($=\cos \theta_i$) is the directional cosine, η_i ($=z_i/\Lambda_i$) the nondimensional z coordinate, and ξ_i ($=d_i/\Lambda_i$) the nondimensional layer thickness of the i th layer. The local heat flux in the z direction can be obtained from²⁶

$$\begin{aligned} q_i(\eta_i) &= \int_{4\pi} I_i \cos \theta_i d\Omega_i \\ &= 2\pi \int_0^1 [i_i^+(\eta_i, \mu_i) - i_i^-(\eta_i, -\mu_i)] \mu_i d\mu_i, \end{aligned} \quad (8)$$

Here $d\Omega_i$ ($=2\pi \sin \theta_i d\theta_i$) is the differential solid angle. The final expression for the heat flux depends on the interface conditions, which determine the coefficients in Eqs. (6) and (7), and the distribution of the intensity gradient dI_{oi}/dt_i . To determine $i_i^+(0, \mu_i)$ and $i_i^-(\xi_i, \mu_i)$ in Eqs. (6) and (7), boundary conditions for phonon scattering at interfaces must be imposed. Our previous papers^{21,23} considered the limiting cases when the interfaces scatter phonons totally specularly and totally diffusely. In the following subsections, boundary conditions for the more general case when the interfaces are partially specular and partially diffuse will be established, followed by a discussion about the interface scattering processes, and an outline of the solution method.

A. Partially diffuse and partially specular scattering interfaces

In this subsection, appropriate boundary conditions for the totally diffuse and the totally specular scattering interfaces

will first be elucidated. The boundary conditions for partially diffuse and partially specular interfaces are established by combining these two cases.

By definition, the phonon intensity leaving a diffuse scattering interface does not depend on direction, thus coefficients $i_i^+(0, \mu_i)$ and $i_i^-(\xi, \mu_i)$ in Eqs. (6) and (7) should be direction independent. Energy balance at the interface between layer $2p$ and layer 1, as shown in Fig. 1, gives

$$\int_{2\pi} I_1^+(0, \mu_1) \mu_1 d\Omega_1 = R_{d12} \int_{2\pi} I_1^-(0, -\mu_1) \mu_1 d\Omega_1 + T_{d21} \int_{2\pi} I_{p2}^+(\xi_2, \mu_2) \mu_2 d\Omega_2, \quad (9)$$

where the integration with respect to the solid angle is over the half space, and R_{dij} and T_{dij} are the energy reflectivity and transmissivity at an interface for phonons incident from the i th layer towards the j th layer, which are direction independent for diffuse interface scattering. The symbol $I_{p2}^+(\xi_2, \mu_2)$ in Eq. (9) represents the phonon intensity corresponding to $\eta_2 = \xi_2$ in the layer preceding layer 1. Because phonons are scattered diffusely at the interfaces, phonons leaving an interface are isotropically distributed, and Eq. (9) can be written as

$$I_1^+(0, \mu_1) = 2R_{d12} \int_{2\pi} I_1^-(0, -\mu_1) \mu_1 d\mu_1 + 2T_{d21} \int_{2\pi} I_{p2}^+(\xi_2, \mu_2) \mu_2 d\mu_2. \quad (10)$$

If phonons are specularly scattered at the interfaces, energy balance can be written down for a differential solid angle,

$$I_1^+(0, \mu_1) \mu_1 d\mu_1 = R_{s12}(\mu_1) I_1^-(0, -\mu_1) \mu_1 d\mu_1 + T_{s21}(\mu_2) I_{p2}^+(\xi_2, \mu_2) \mu_2 d\mu_2, \quad (11)$$

where $R_{s12}(\mu_1)$ and $T_{s21}(\mu_2)$ are the specular reflectivity and transmissivity for phonons incident from layer 1 at angle θ_1 . Angles θ_1 and θ_2 for specular reflection and refraction of phonons obey the Snell law for acoustic waves,

$$\frac{\sin \theta_1}{v_1} = \frac{\sin \theta_2}{v_2}. \quad (12)$$

Strictly speaking, Eq. (11) is valid only for transversely polarized phonons in an isotropic solid experiencing elastic-scattering processes at the interface. For longitudinal phonons or transverse phonons polarized in the plane of incidence, mode conversion at the interface can occur, leading to three transmitted and three reflected phonon waves in an anisotropic crystal or two transmitted and two reflected waves in an isotropic crystal.²⁸ Consideration of such a mode conversion would require modification of Eq. (11) to include each of the transmitted and reflected phonon branches. This would make the solution of the BTE much more difficult. In addition, we are also interested in considering the inelastic scattering of phonons at interfaces, for which there exist no simple relations among angles of the incident, transmitted,

and reflected phonons. An approximate relation will be proposed in the inelastic acoustic mismatch model presented in Sec. II B. Due to the approximate nature of these models in dealing with the phonon-scattering processes at the interface, we will neglect phonon mode conversion at interfaces. There are reasons to believe that the neglecting of the mode conversion does not introduce a large error and alter the conclusion of this work. In a recent work,²⁹ we modeled the phonon transmission through a single film including the mode conversion, but neglecting internal scattering and assuming only elastic scattering at interfaces. The results show that the transverse phonons polarized both in and perpendicular to the plane of incidence contribute nearly equally to the film thermal conductivity. The assumption of no mode conversion for longitudinal phonons may lead to an overestimation of the phonon transmission. It will be shown, however, that the specular, elastic-scattering model underestimates the superlattice thermal conductivity. A correction for the overestimation of the longitudinal phonon transmissivity will make the calculated thermal conductivity even lower. To explain the experimental data, inelastic phonon scattering must be postulated to occur at the interfaces. For the inelastic-scattering process, only approximate relations among the angles of incident, transmitted and reflected waves can be established, as stated above.

If the interfaces scatter phonons partially specularly and partially diffusely, the corresponding boundary conditions can be obtained by combining Eqs. (10) and (11),

$$I_1^+(0, \mu_1) = p \{ R_{s12}(\mu_1) I_1^-(0, -\mu_1) + t_{s21}(\mu_2) I_{p2}^+(\xi_2, \mu_2) \} + 2(1-p) \left\{ R_{d12} \int_{2\pi} I_1^-(0, -\mu_1) \mu_1 d\mu_1 + T_{d21} \int_{2\pi} I_{p2}^+(\xi_2, \mu_2) \mu_2 d\mu_2 \right\}, \quad (13)$$

where p is the interface specularity parameter,¹⁵ representing the fraction of phonons experiencing specular scattering at the interface, and t_{s21} is related to T_{s21} by

$$t_{s21}(\mu_2) = T_{s21}(\mu_2) \mu_2 d\mu_2 / (\mu_1 d\mu_1). \quad (14)$$

Similar consideration on the energy balance at the two other interfaces forming one period of a superlattice yields

$$I_1^-(\xi_1, -\mu_1) = p \{ R_{s12}(\mu_1) I_1^+(\xi_1, \mu_1) + t_{s21}(\mu_2) I_2^-(0, -\mu_2) \} + 2(1-p) \times \left\{ R_{d12} \int_{2\pi} I_1^+(\xi_1, \mu_1) \mu_1 d\mu_1 + T_{d21} \int_{2\pi} I_2^-(0, -\mu_2) \mu_2 d\mu_2 \right\}, \quad (15)$$

$$I_2^+(0, \mu_2) = p \{ R_{s21}(\mu_2) I_2^-(0, -\mu_2) + t_{s12}(\mu_1) I_1^+(\xi_1, \mu_1) \} \\ + 2(1-p) \left\{ R_{d21} \int_{2\pi} I_2^-(0, -\mu_2) \mu_2 d\mu_2 \right. \\ \left. + T_{d12} \int_{2\pi} I_1^+(\xi_1, \mu_1) \mu_1 d\mu_1 \right\}, \quad (16)$$

$$I_2^-(\xi_2, -\mu_2) = p \{ R_{s21}(\mu_2) I_2^+(\xi_2, \mu_2) \\ + t_{s12}(\mu_1) I_{n1}^-(0, -\mu_1) \} + 2(1-p) \\ \times \left\{ R_{d21} \int_{2\pi} I_2^+(\xi_2, \mu_2) \mu_2 d\mu_2 \right. \\ \left. + T_{d12} \int_{2\pi} I_{n1}^-(0, -\mu_1) \mu_1 d\mu_1 \right\}, \quad (17)$$

where $I_{n1}^-(0, -\mu_1)$ represents the phonon intensity corresponding to $\eta_1 = 0$ in the layer next to layer 2. The above set of interface conditions is generally applicable to multilayer structures, and is not subject to the periodicity requirement of superlattices. For a periodic structure with heat flow in the z direction, temperatures at the corresponding locations of two identical layers, and thus the equilibrium intensities $I_{p02}^+(\xi_2)$ and $I_{o2}^+(\xi_2)$ do not equal to each other. We argue, however, that the angular distribution of the deviation function, i , must be similar between identical layers of a superlattice,²¹ i.e., $i_{pi}(\eta_i, \mu_i) = K i_i(\eta_i, \mu_i)$, where K is a similarity constant. Substituting this similarity relation into Eq. (8), it becomes clear that K must equal 1 when there is no internal heat generation. The above reasoning leads to

$$i_{p2}(\eta_2, \mu_2) = i_2(\eta_2, \mu_2) \quad \text{and} \quad i_{n1}(\eta_1, \mu_1) = i_1(\eta_1, \mu_1) \quad (18)$$

Based on the four boundary conditions, Eqs. (13) and (15)–(17), the unknown coefficients $i_i^+(0, \mu_i)$ and $i_i^-(\xi_i, -\mu_i)$ in Eqs. (6) and (7) can, in principle, be expressed in terms of the unknown equilibrium phonon distributions $I_{01}(\eta_1)$ and $I_{02}(\eta_2)$ and their derivatives. Expressions for the case of totally diffuse scattering interface have been published before, and are very complicated.²¹ After the coefficients in Eqs. (6) and (7) are determined, these two equations can be substituted into Eq. (8) to yield two governing equations for the temperature distribution and the interface temperature drop. For partially diffuse interfaces, however, no explicit expressions, no matter how complex, can be obtained for the unknown coefficients in Eqs. (6) and (7). It is found that the previously established methods^{21,23} for totally diffuse and totally specular scattering interfaces are difficult to apply to the partially diffuse and partially specular interfaces. A solution method is thus developed. Before describing this method, the phonon reflection and transmission processes at interfaces and the associated TBR phenomenon will first be discussed.

B. Interface properties and thermal boundary resistance

The above formulation indicates that phonon transfer across superlattices depends on the interface transmissivity and reflectivity. These interface properties have been studied

extensively related to the work on the TBR.^{30,31} Despite those studies, quantitative predictions of the TBR are still not satisfactory when compared with experimental results.³² One possible explanation of the poor agreement between modeling and experimental results lies in the difficult of controlling the interfaces. Most existing experimental studies were performed on interfaces formed by mechanically joining two materials or by deposition of polycrystalline films onto a substrate. Interface structures thus formed can deviate significantly from the assumptions underlying the models. The nearly perfect interfaces in superlattice structures offer an ideal system to study TBR. In this work, two existing extreme models on the TBR, with proper modifications, will be employed in evaluating the interface reflectivity and transmissivity. These two models are the acoustic mismatch model³⁰ and the diffuse scattering model.³¹ Predictions based on the acoustic mismatch model have been relatively successful at very low temperatures where heat transfer is dominated by long-wavelength phonons. At higher temperatures, where most phonons have short wavelengths, the diffuse scattering limit model developed by Swartz and Pohl³¹ may be more appropriate.

1. Diffuse scattering limit

The diffuse scattering limit model³¹ is established based on the assumption that phonons experiencing scattering at the interface totally lose their memory on the side which they come from. In this case, there is no way to tell whether a phonon leaving the interface is due to reflection from the same side or transmission from the other side; hence

$$T_{dji} = R_{dij} = 1 - T_{dij}. \quad (19)$$

The second equality in the above relations comes from the energy conservation requirement. When both sides of the interface are at the same temperature, the principle of energy balance requires

$$T_{d12} \int_{2\pi} I_{o1}(T) \cos \theta_1 d\Omega_1 = T_{d21} \int_{2\pi} I_{o2}(T) \cos \theta_2 d\Omega_2. \quad (20)$$

At low temperatures, the integration limit in Eq. (1) can be extended to infinity. Substituting Eq. (1) into Eq. (20) leads to the following expression for the phonon transmissivity:³¹

$$T_{dij} = \frac{\sum_m v_{mj}^{-2}}{\sum_m v_{mi}^{-2} + \sum_m v_{mj}^{-2}}, \quad (21)$$

where v_{mi} is the magnitude of the phonon group velocity of the m branch (m is transverse or longitudinal) in the i th layer. When the temperature is high, the above relation is no longer valid. A similar relation can be obtained by utilizing the relation between intensity and specific heat,²⁵

$$\frac{dI_o}{dT} = \frac{1}{4\pi} \sum_m \int v_m h \nu D(\nu) \frac{df_o}{dT} d\nu = \frac{vC}{4\pi}. \quad (22)$$

Assuming that the temperature variation across superlattices is small and the specific heat can be treated as a constant in this temperature range, the intensity can be written as

$$I_o = \frac{vC(T - T_{\text{ref}})}{4\pi}, \quad (23)$$

where T_{ref} is a reference temperature. From Eqs. (19), (20), and (23), the following expression for phonon transmissivity at the totally diffuse scattering limit is obtained:

$$T_{dij} = \frac{C_j v_j}{C_i v_i + C_j v_j}. \quad (24)$$

In deriving Eq. (24), it is assumed that phonons of all frequencies can transmit through the interface. This assumption implies that scattering at the interface can be inelastic, i.e., phonons in one layer with frequency higher than the maximum frequency of phonons in the adjacent layers can transmit into adjacent layers by splitting into two or more phonons through anharmonic interatomic interactions. In the diffuse scattering model, these inelastic-scattering processes redistribute phonons isotropically in all directions.

2. Elastic acoustic mismatch model

From the acoustic mismatch theory, the interface reflectivity and transmissivity for specular interfaces can be expressed as³⁰

$$R_{s12}(\mu_1) = \left| \frac{Z_1 \mu_1 - Z_2 \mu_2}{Z_1 \mu_1 + Z_2 \mu_2} \right|^2 \quad (25)$$

and

$$T_{s12}(\mu_1) = \frac{4Z_1 Z_2 \mu_1 \mu_2}{(Z_1 \mu_1 + Z_2 \mu_2)^2}, \quad (26)$$

where $Z_i = \rho_i v_i$ is the acoustic impedance of the i th layer. The above expressions neglect possible phonon mode conversion, as stated above. Another restriction on the validity of the above two equations is that the interface scattering is an elastic scattering process, i.e., the reflected and transmitted phonons are at the same frequency as the incident phonons. In this case, the following reciprocal relations for the spectral reflectivity and transmissivity are valid: $R_{s12}(\mu_1) = R_{s21}(\mu_2)$ and $T_{s12}(\mu_1) = T_{s21}(\mu_2)$. These relations hold true for the spectrally integrated interface properties only if the incident phonons from both sides have identical spectra. In real superlattices, however, the phonon spectra in two layers are seldom identical. Without loss of generality, it is assumed here that the maximum acoustic-phonon frequency in layer 2 is higher than that in layer 1. Phonons in layer 2 with frequencies above the maximum acoustic-phonon frequency in layer 1 are confined in layer 2 if only elastic scattering is allowed at the interfaces. This phonon confinement effect has been studied extensively in literature.¹³ Since the phonon confinement occurs inside the second layer, Eqs. (25) and (26) are valid for the spectrally integrated reflectivity and transmissivity in the first layer. The total phonon transmissivity from layer 2 into layer 1 can be related to T_{12} based on the energy balance requirement for a differential solid angle. If phonons at the two sides of an interface are at an equal temperature and the interfaces are totally specular, Eq. (11) yields

$$T_{s12}(\mu_1) I_{o1}(T) = t_{s21}(\mu_2) I_{o2}(\mu_2). \quad (27)$$

Based on Eqs. (12) and (23), Eq. (27) can be written as

$$T_{s21}(\mu_2) = \frac{T_{s12}(\mu_1) I_{o1}(T) \mu_1 d\mu_1}{I_{o2}(\mu_2) \mu_2 d\mu_2} = \frac{C_1 v_1^3}{C_2 v_2^3} T_{s12}(\mu_1). \quad (28)$$

Equations (24)–(28) are valid when the angle of incidence is less than the critical angle. Above the critical angle, total internal reflection occurs, and we have

$$R_{s12}(\mu_1) = 1, \quad T_{s12}(\mu_1) = 0. \quad (29)$$

3. Inelastic acoustic mismatch model

The above elastic acoustic mismatch model takes into consideration the phonon confinement effect by modifying the transmissivity for confined phonons. Studies by Stoner and Maris³² suggest that inelastic scattering should be included to explain some of their experimental data on the TBR between solids at high temperatures. Although Eq. (24) has included the inelastic-scattering effect in the diffuse scattering limit model, the model neglects the possibility that certain directional properties of the incoming phonons are persevered during the inelastic-scattering process. To model the inelastic-scattering processes at interfaces, Stoner and Maris³² used lattice-dynamic simulations by assuming an interfacial atomic layer with a different interatomic potential from those of the bulk materials. Here we propose a simple analytical model to account for the inelastic-scattering processes that preserve the direction of incident phonons.

For elastic scattering processes, the Snell law [Eq. (12)], is satisfied. For inelastic-scattering processes such as three-phonon scattering, the wave vectors of other two involved phonons will no longer obey the Snell law but in principle can be calculated. As an approximate treatment, we can use an average angle of refraction for these two phonons. The relation between the refraction angle and the incident angle can be obtained from Eq. (27) by requiring that the transmissivity T_{12} must equal to T_{21} . This leads to

$$\frac{\mu_2 d\mu_2}{\mu_1 d\mu_1} = \frac{C_1 v_1}{C_2 v_2} \quad \text{or} \quad \frac{\sin \theta_1}{\sin \theta_2} = \left(\frac{C_2 v_2}{C_1 v_1} \right)^{1/2}. \quad (30)$$

In the low-temperature limit, the specific heat C is proportional to v^{-3} and the above relation reduces to Eq. (12). We will use Eq. (30), combined with Eqs. (25) and (26) to calculate the reflectivity and transmissivity and call this the inelastic acoustic mismatch model.

4. Thermal boundary resistance

After the transmissivity at the interface is known, the TBR can be determined. The prevailing model accepted for the TBR, as shown in Fig. 2(a), bears a strict analogy with radiative transfer.³¹ Assuming that the phonon MFP in each

solid is infinite and that phonons at temperature T_{e1} or T_{e2} are emitted by the solid on each side, the following relation between the heat flux and the temperature drop can be obtained,

$$q = \int_{2\pi} T_{12}(\mu_1) I_{o1}(T_{e1}) \cos \theta_1 d\Omega_1 - \int_{2\pi} T_{21}(\mu) I_{o2}(T_{e2}) \cos \theta_2 d\Omega_2. \quad (31)$$

In the totally diffuse limit, the above equation gives

$$q = T_{d12} C_1 v_1 \Delta T_{e12} / 4, \quad (32)$$

where ΔT_{e12} is the temperature difference between those of the emitted phonons.

For totally specular interfaces, Eq. (31) becomes

$$q = \frac{C_1 v_1 \Delta T_{e12}}{2} \int_{2\pi} T_{s12}(\mu_1) \mu_1 d\mu_1. \quad (33)$$

From the above relation, the TBR can be expressed as

$$W_e = \frac{\Delta T_{e12}}{q} = \begin{cases} \frac{4}{T_{d12} C_1 v_1} & \text{diffuse limit} \\ \frac{2}{C_1 v_1 \int T_{s12}(\mu_1) \mu_1 d\mu_1} & \text{specular limit.} \end{cases} \quad (34)$$

The above definition for TBR is based on the temperature of the emitted phonons. For heat conduction in very thin films, the local thermodynamic condition is far from equilibrium, and temperature loses its conventional meaning of representing a thermal equilibrium state.^{25,31} In the current work, temperature is a representation of the average energy of all phonons around a local point, and is equivalent to the equilibrium temperature of those phonons if they redistribute adiabatically to an equilibrium state. This temperature definition is inconsistent with the above definition for the TBR based on the temperature of emitted phonons because as illustrated in Figs. 2(a) and 2(b), the equivalent equilibrium temperature on each side is different from that of the emitted phonons. A more consistent picture of TBR is provided by Simons³³ based on the equivalent equilibrium temperature of phonons on each side of the interface. It can be shown that the equivalent equilibrium temperature, T_1 and T_2 , can be expressed in terms of T_{e1} and T_{e2} as

$$T_1 = T_{e1} - (T_{e1} - T_{e2}) \int T_{12}(\mu_1) \mu_1 d\mu_1$$

and

$$T_2 = T_{e2} + (T_{e1} - T_{e2}) \int T_{21}(\mu_2) \mu_2 d\mu_2, \quad (35)$$

such that

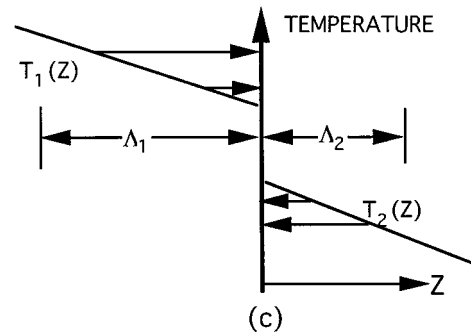
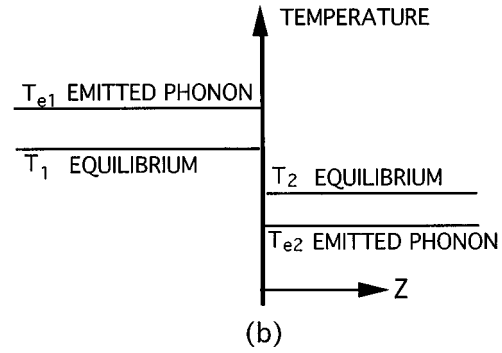
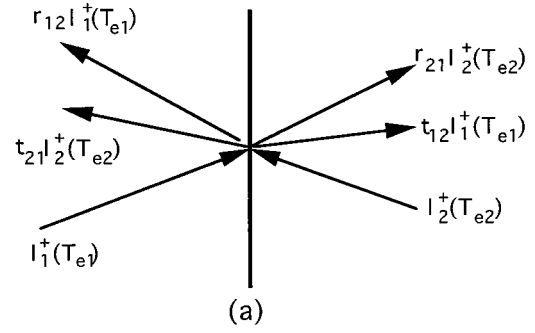


FIG. 2. Interpretation of thermal boundary resistance: (a) phonon reflection and transmission, (b) equilibrium and emitted phonon temperature for infinite phonon mean free path, and (c) effect of the finite phonon mean free path.

$$T_1 - T_2 = \Delta T_{12} = \left[1 - \int T_{12}(\mu_1) \mu_1 d\mu_1 - \int T_{21}(\mu_2) \mu_2 d\mu_2 \right] (T_{e1} - T_{e2}). \quad (36)$$

By defining the TBR based on the difference of the equivalent equilibrium temperature, ΔT_{12} , the classical paradox on the existence of a finite TBR for an imaginary interface in the same material³⁰ can be eliminated. This is because when $T_{12} = T_{21} = 1$, Eq. (36) leads to $\Delta T_{12} = 0$. Based on ΔT_{12} rather than ΔT_{e12} , the following expressions for the TBR are obtained:

$$W = \frac{\Delta T_{12}}{q} = \begin{cases} \frac{4[1 - 0.5(T_{d12} + T_{d21})]}{T_{d21}C_2v_2} & \text{diffuse limit} \\ \frac{2 \left[1 - \int T_{s12}(\mu_1)\mu_1 d\mu_1 - \int T_{s21}(\mu_2)\mu_2 d\mu_2 \right]}{C_1v_1 \int T_{s12}(\mu_1)\mu_1 d\mu_1} & \text{specular limit.} \end{cases} \quad (37)$$

It should be emphasized that both the classical definition [Eq. (34)] and the temperature consistent definition [Eq. (37)] lead to the correct result for heat flux. Which definition is more appropriate depends on the actual experimental configuration, i.e., whether the temperature sensor measures the temperature of emitted phonons or the equivalent equilibrium temperature of all the phonons on each side.³⁴ For heat-transfer calculations involving both conduction inside a medium and the TBR at an interface, the equivalent equilibrium temperature is clearly a more appropriate choice.

C. Method of numerical solution

The four boundary conditions in Eqs. (13) and (15)–(17), plus Eqs. (6) and (7), involve a total of eight equations but ten unknowns: the eight forward and backward intensities at the interfaces, and the distribution of the effective temperature in each layer. In this work, it is assumed that no internal heat generation occurs in the medium; thus the heat flux as given by Eq. (8) is a constant. By normalizing temperature to the heat flux, two additional equations are obtained. In principle, the intensity distribution at the boundaries as well as the normalized temperature distribution in each layer can be determined from this set of equations.

Clearly, exact analytical solutions of these equations are impossible. So far, we have reported numerical results for two special cases, i.e., when the interfaces are totally diffuse and totally specular.^{21,23} Numerical solutions for these two cases are obtained by eliminating the unknown intensities at the interfaces and solving two integral equations governing the nondimensional temperature distributions in one period. For the partially diffuse and partially specular interfaces, elimination of all the intensities is impossible. We have attempted to solve the equations simultaneously by discretizing the integrals using the Gauss-Legendre quadrature. Numerical instability was encountered in these attempts.

A new method of solution is developed here based on the symmetry implied by the governing equations and the corresponding boundary conditions. As shown in the Appendix, the following antisymmetric relations exist:

$$i_j^+(0, \mu_j) = -i_j^-(\xi_j, -\mu_j)$$

and

$$i_j^+(\xi_j, \mu_j) = -i_j^-(0, -\mu_j). \quad (38)$$

Using these relations and Eqs. (7) and (8), the boundary conditions can be written as

$$\begin{aligned} & [1 + pR_{s12}(\mu_1)e^{-\xi_1/\mu_1}]i_1^+(0, \mu_1) - pT_{s21}(\mu_2)e^{-\xi_2/\mu_2}i_2^+(0, \mu_2) + 2(1-p)R_{d12} \int_0^1 e^{-\xi_1/\mu_1}i_1^+(0, \mu_1)\mu_1 d\mu_1 \\ & - 2(1-p)T_{d21} \int_0^1 e^{-\xi_2/\mu_2}i_2^+(0, \mu_2)\mu_2 d\mu_2 - pR_{s12}(\mu_1)\Pi_1 \int_0^{\xi_1} G_1(t_1)e^{-(\xi_1-t_1)/\mu_1} dt_1 \\ & + pT_{s21}(\mu_2) \int_0^{\xi_2} G_2(t_2)e^{-(\xi_2-t_2)/\mu_2} dt_2 - 2(1-p)R_{d12}\Pi_1 \int_0^{\xi_1} G_1(t_1)E_3(\xi_1-t_1) dt_1 \\ & + 2(1-p)T_{d21} \int_0^{\xi_2} G_2(t_2)E_3(\xi_2-t_2) dt_2 = \Psi_{21}\Pi_1 [pT_{s12}(\mu_1) + (1-p)T_{d12}], \end{aligned} \quad (39)$$

where i_i , G_i , and Ψ_{ij} are normalized intensity, temperature gradient distribution, and TBR, respectively, which are defined as

$$i_i = \frac{\pi i_i}{q}, \quad G_i = \frac{C_2 v_2}{4q} \frac{dT_i(t_i)}{dt_i}, \quad \Psi_{ij} = \frac{C_2 v_2 \Delta T_{ij}}{4q}, \quad (40)$$

and Π_i are

$$\Pi_1 = C_1 v_1 / (C_2 v_2) \quad \text{and} \quad \Pi_2 = 1, \quad (41)$$

The exponential integral function E_n ($n=3$) in Eq. (39) is defined as²⁶

$$E_n(t) = \int_0^1 \mu^{n-2} e^{-t/\mu} d\mu. \quad (42)$$

A similar equation can be obtained by permuting the subscript indices 1 and 2 in Eq. (39). Using these two equations,

the number of unknown intensity distribution at the interfaces is reduced from eight to two. Two additional equations can be obtained from Eq. (8),

$$\int_0^1 (e^{-\eta_i/\mu_i} + e^{-(\xi_i - \eta_i)/\mu_i}) \iota_i^+(0, \mu_i) \mu_i d\mu_i - \Pi_i \int_0^{\xi_i} G_i(t_i) E_3(|\eta_i - t_i|) dt_i = \frac{1}{2}, \quad (43)$$

where $i=1$ and 2 .

The above integral equations [Eqs. (39) and (43)] can be solved numerically to yield the intensity distribution at the interfaces, the TBR, and the nondimensional temperature distributions. The Gauss-Legendre integration scheme is used here to approximate the integrals in Eqs. (39) and (43). In doing such a discretization, two complications arise. One is due to the fact that the roots of the Gauss quadrature depend on the integration interval and the number of integration points. Such roots in layers 1 and 2 will not satisfy the Snell law as given by Eq. (12), while the directional cosines μ_1 and μ_2 in Eq. (39) are related to each other according to the Snell law. To overcome this problem, discretization must also be carried out for those angles that are conjugated, through the Snell law, to the angles in the adjacent layers as determined by the Gauss quadrature. Thus, if the n th-order Gauss quadrature is used, a total of $4 \times n$ discrete equations must be written down for $\iota_1^+(0, \mu_1)$ and $\iota_2^+(0, \mu_2)$. The second complication is due to the occurrence of the total internal reflection. At the critical point, the reflectivity and transmissivity vary drastically. This sharp variation requires the separation of integration over angle into two parts for the layer in which the total internal reflection occurs, as demarcated by the critical angle. A total of $6 \times n$ discretized equations is thus used for the intensity distributions $\iota_1^+(0, \mu_1)$ and $\iota_2^+(0, \mu_2)$. In addition, the discretization over the distribution of nondimensional temperature gradient G will give $2 \times m$ sets of discretized equations, for an m th-order Gauss quadrature in the η -coordinate direction. Two more discrete equations can be obtained by setting $\eta_i=0$ in Eq. (39) or (43), to

compensate for the two additional unknowns related to the TBR, Ψ_{ij} . The final total number of discretized equations is $6 \times n + 2 \times m + 2$, with $6 \times n$ unknowns in intensity, $2 \times m$ unknowns in the nondimensional temperature gradient distribution, and two unknowns in the nondimensional thermal boundary resistance. Direct matrix inversion is employed to obtain the final solution for ι_i , G_i , and Ψ_{ij} , followed by integration of G_i to yield the nondimensional temperature distribution in each layer. The accuracy of the results is tested by doubling the number of integration points. Another way to check the results is to investigate their asymptotic behavior. In the limit where each layer is thick compared to the MFP, the Fourier law should be valid. Combining Eqs. (3) and (40) leads to the following asymptotic solution

$$\lim_{\xi_i \rightarrow \infty} G_i(t_i) = -3/4\Pi_i. \quad (44)$$

D. Approximate solutions

As will be shown by the numerical results in Sec. III, most of the temperature drop across the superlattice occurs at the interfaces when the layers are very thin. Based on this observation, approximate analytical solutions for the effective thermal conductivity of superlattices can be obtained by neglecting the temperature drop inside the film, and assuming that the effective thermal conductivity of superlattices is dominated by the interface TBR. Under this approximation, in dimensional form, Eq. (39) becomes

$$(1 + pR_{s12})i_1^+ - pt_{s21}i_2^+ = \{C_1 v_1 \Delta T_{12} [pT_{s12} + (1-p)T_{d21}] + 2(1-p)[T_{d12} - R_{d21}]q\}/4\pi, \quad (45)$$

and a similar equation is obtained by permuting the subscript indices. Solving the above equations for i_1^+ and i_2^+ , and substituting the solutions back into Eq. (8), yields an expression for the heat flux, from which the effective thermal conductivity can be expressed as

$$k_e = \frac{0.5(d_1 + d_2)C_2 v_2 \int_0^1 \{2pT_{s21} + (1-p)T_{d21}[1 + pR_{s12} + pt_{s12}]/D(\mu_2)\} \mu_2 d\mu_2}{1 - 2(1-p) \int_0^1 \{[(1 + pR_{s12})(-R_{d21} + T_{d12}) + pt_{s12}(-R_{d12} + T_{d21})]/D\} \mu_2 d\mu_2}, \quad (46)$$

where

$$D(\mu_1) = (1 + pR_{s21})(1 + pR_{s12}) - p^2 T_{s12} T_{s21}. \quad (47)$$

For totally specular interfaces, the above equation is simplified to

$$k_e = (d_1 + d_2)C_2 v_2 \int_0^1 \frac{T_{s21}(\mu_2) \mu_2 d\mu_2}{[1 + R_{s12}(\mu_1)][1 + R_{s21}(\mu_2)] - T_{s12}(\mu_1) T_{s21}(\mu_2)}. \quad (48)$$

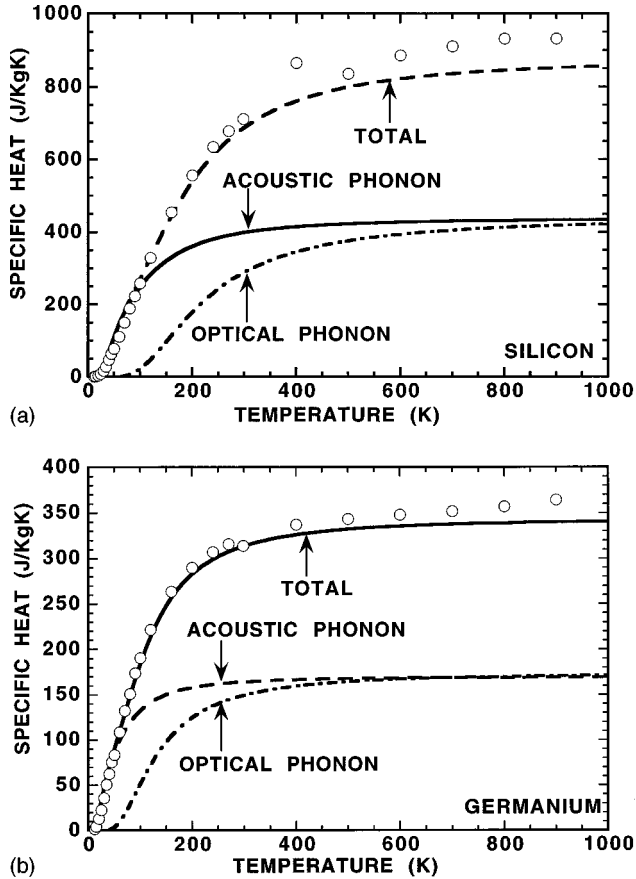


FIG. 3. Specific heat of (a) Si and (b) Ge, showing contributions from different phonon modes.

For totally diffuse interfaces under the diffuse scattering limit, Eq. (46) leads to

$$k_{de} = 0.5(d_1 + d_2)C_1v_1T_{d12}. \quad (49)$$

E. Specific heat, group velocity, and phonon mean free path

The above models need several bulk material properties as input parameters, including the specific heat, the phonon group velocity, and the phonon MFP. The simplest method to calculate the bulk phonon MFP is from Eq. (3) based on the speed of sound, the bulk thermal conductivity, and the specific heat. This method, however, neglects the fact that at room temperature most phonons are populated close to the zone boundary where the phonon group velocity is significantly smaller than the sound velocity. In addition, a significant portion of the specific heat is due to optical phonons that contributes little to heat transfer.^{35,36} A better estimation of the phonon MFP and the group velocity can be obtained from a more realistic approximation of the phonon dispersion relations.^{15,20} In a previous paper,¹⁵ we have shown that the specific heat of GaAs can be calculated without any fitting parameters (including the Debye temperature) by approximating the dispersion of the transverse and the longitudinal-acoustic phonons with simple sine functions. Similar calculations have been done for silicon and germanium. Figures 3(a) and 3(b) demonstrate the satisfactory agreement between the calculated and listed specific-heat data of Si and Ge. At room temperature, about one-third of

TABLE I. Room-temperature properties used in the calculation of the thermal conductivity of GaAs/AlAs and Si/Ge superlattices.

Material	Model	Specific heat $\times 10^6$ J/m ³ K	Group velocity m/s	Mean free path Å
GaAs	Debye	1.71	3700	208
	Dispersion	0.88	1024	1453
AlAs	Debye	1.58	4430	377
	Dispersion	0.88	1246	2364
Si	Debye	1.66	6400	409
	Dispersion	0.93	1804	2604
Ge	Debye	1.67	3900	275
	Dispersion	0.87	1042	1986

the specific heat of Si is due to optical phonons, and, for Ge, the optical-phonon contribution accounts for about one-half of the total specific heat. Since optical phonons have a very low group velocity, we will neglect their contribution to the bulk thermal conductivity as well as to the superlattice. In addition to excluding the optical phonons, the phonon group velocity is also calculated from approximate dispersion relations weighed over the model specific heat.¹⁵ Table I lists the phonon properties based on the two estimation methods, i.e., the method based on the speed of sound and the total specific heat (Debye model), and the method based on a sine function approximation to each acoustic-phonon polarization and the exclusion of the optical phonons (dispersion model).¹⁵

III. RESULTS AND DISCUSSION

Sample calculations are carried out for GaAs/AlAs and Si/Ge superlattices. Figures 4(a)–4(c) show the distributions of the nondimensional temperature gradient, and Figs. 5(a)–5(c) the distributions of nondimensional temperature in two adjacent layers of GaAs/AlAs superlattices. For large layer thickness [Figs. 4(a) and 5(a)], the gradient distribution approaches a constant of $-\frac{3}{4}$ in layer 2 and -0.825 ($=3/4\Pi_1$) in layer 1 over a large portion of each layer, in agreement with the Fourier heat conduction theory, i.e., Eq. (44). Near the interfaces, the temperature gradient increases sharply, reflecting the nonequilibrium nature of the transport process near the interface as shown in Fig. 2(a). In this case, the majority of temperature drop occurs inside the layer and the interface conditions have little effect on the overall temperature drop [Fig. 5(a)]. For small layer thickness, say a 100-Å period superlattice, the temperature gradient becomes more nonuniform and its value deviates from the Fourier results. For totally specular interfaces, large differences exist in the TBR and the distribution of the temperature gradient between results obtained from the elastic acoustic mismatch [Figs. 4(b) and 5(b)] and inelastic acoustic mismatch [Figs. 4(c) and 5(c)] models. Under the elastic acoustic mismatch model, phonons are confined in the AlAs layer and a large temperature drop occurs at the interface due to the reduced phonon transmissivity. For inelastic scattering at interfaces, phonons are not confined, and, correspondingly, only a small temperature drop develops at a totally specular scattering interface. Similar results have been obtained for Si/Ge superlattices. Because the mismatch in the specific heat and group velocity is larger between Si and Ge than between GaAs and

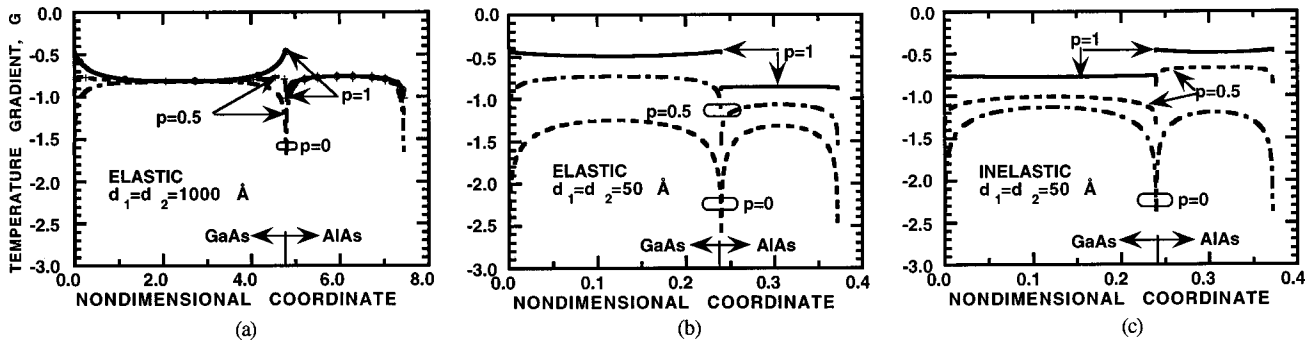


FIG. 4. Distributions of the nondimensional temperature gradient in one period of GaAs/AlAs superlattices with equal thickness layers under different interface scattering models; (a) $d_1 = d_2 = 1000 \text{ \AA}$, (b) $d_1 = d_2 = 50 \text{ \AA}$, and (c) $d_1 = d_2 = 50 \text{ \AA}$, where (a) and (b) are based on elastic acoustic mismatch model for contributions from specular scattering processes, and (c) is based on inelastic acoustic mismatch model.

AlAs, the temperature drop at a Si/Ge interface is larger than that at a GaAs/AlAs interface.

The distribution of the normalized intensity deviations at two interfaces is shown in Figs. 6(a)–6(d) for GaAs/AlAs superlattices. Figures 6(a) and 6(b) are results based on the elastic-acoustic-mismatch model, while Figs. 6(c) and 6(d) are results based on the inelastic acoustic mismatch model. The total internal reflection occurs in GaAs under the elastic acoustic mismatch model [Fig. 6(a)], but changes to the AlAs layer under the inelastic-scattering model [Fig. 6(d)]. This switching is a consequence of modifying the Snell law according to Eq. (30). In interpreting the angular distributions of the normalized intensity deviations, it should be kept in mind that they represent the deviation from the equilibrium intensity. A positive value means phonons contribute to the energy flow in the heat flux direction, and vice versa. When the incident angle is smaller than the critical angle, the intensity decreases monotonously with increasing angle of incidence. Above the critical angle, the deviation in intensity increases with angle, due to scattering of phonons inside the layer into these directions. For diffuse interfaces, the distribution of intensity is isotropic, as expected.

Figures 7(a)–7(d) illustrate the behavior of the TBR as a function of the layer thickness. First, it should be emphasized that numerical solution indeed shows that the TBR is independent of the phonon incident direction, i.e., $\Psi_{12} = \Psi_{21}$, as required by symmetry. Second, the TBR also becomes thickness dependent. Third, the TBR calculated for thick films does not approach the limit as given in Eq. (37). The reason for this latter discrepancy lies in the temperature nonuniformity near the interface. The previous derivation of the TBR assumes that the phonon MFP is infinite, and thus the inci-

dent phonons from each side will be at one uniform temperature, as illustrated in Fig. 2(b). When the phonon MFP is a finite value, all phonons within the range of the order of one MFP can reach the interface ballistically and thus affect the TBR. Equation (37) defines the TBR based on the temperatures of phonons exactly at the two sides of an interface. Figure 2(c) shows, however, that phonons away from the interface but within the range of one MFP participate in the energy exchange across the interfaces directly. This means that the TBR depends on the temperature gradient in the media. For superlattices, the temperature gradient is further related to layer thickness, leading to the dependence of the TBR on the film thickness. Such a thickness dependence of the TBR is similar to the separation dependence of the electrical conductance of two constrictions in parallel³⁷ or in series.³⁸ Both are due to the influences of the interfaces or constrictions to the distributions of the incident phonons or electrons. Quantum interference of electron waves is the cause of the incident electron wave redistribution in the cited references, while the thickness dependence of the TRB discussed here is caused by the phonon density change in thin films.

To understand heat conduction mechanisms in superlattices further, the effective thermal conductivity of superlattice structures will be calculated and compared with recent experimental results on GaAs/AlAs (Ref. 5) and Si/Ge superlattices.⁷ All of the above calculations are performed based on the bulk specific heat and the speed of sound (values listed under the Debye model in Table I). Since the presented temperature distributions are normalized to the product of the specific heat and the group velocity, these results should not change much even when the optical-phonon con-

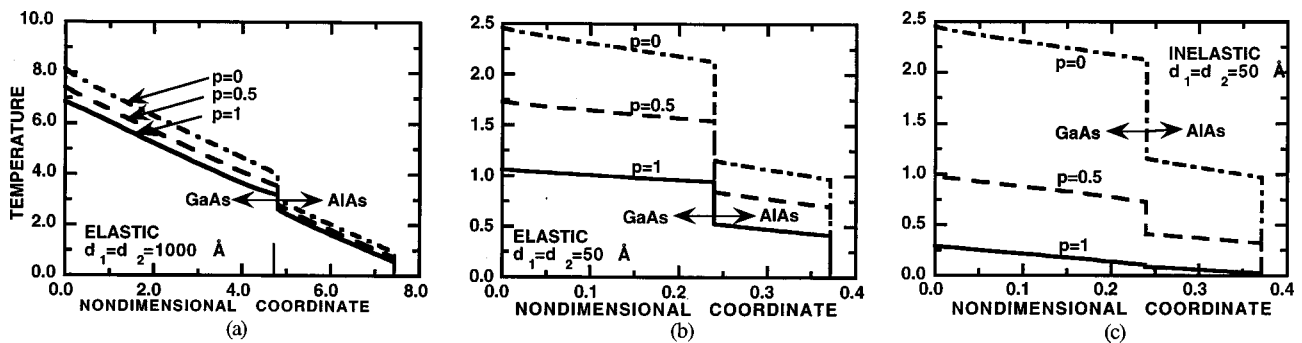


FIG. 5. Nondimensional temperature distribution for the corresponding superlattices in Figs. 4(a)–4(c).

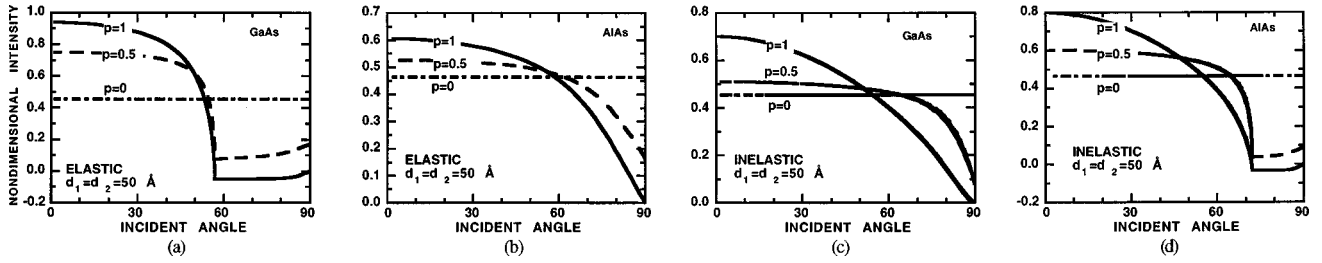


FIG. 6. Distribution of nondimensional intensity in the forward direction at $\eta=0$ as a function of polar angle; (a) and (b) are results based on elastic acoustic mismatch model, and (c) and (d) are based inelastic acoustic mismatch model; (a) and (d) represent the layer in which total internal reflection occurs.

tribution is excluded and an average phonon group velocity is used (values listed under the dispersion model in Table I). For the thermal conductivity modeling, however, we must be more discriminative on the values of the specific heat and the phonon group velocity used in the calculations. Table I lists two groups of properties for each material. One is based on the total specific heat and the average of the sound velocity, and the other is based on the specific heat of the acoustic phonons only and a group velocity averaged over the first Brillouin zone. Modeling results based on both groups of properties will be discussed.

Figures 8(a)–8(d) show the modeling results on the thickness dependence of the thermal conductivity of GaAs/AlAs superlattices that are calculated under different conditions, and compare them with experimental results of Capinski and Maris.⁵ Figures 9(a)–9(d) illustrate a similar comparison with Si/Ge superlattices.⁷ The specular reflectivity and transmissivity in Figs. 8(a), 8(b), 9(a), and 9(b) are based on the elastic acoustic phonon mismatch model, and thus include the phonon confinement effect. The differences among these figures are in the values of the specific heat and the phonon group velocity. Figures 8(a) and 9(a) represent the case where no consideration is given to the phonon dispersion and the effect of optical phonons on the specific heat, while Figs. 8(b) and 9(b) are calculated with these two factors taken into consideration. Although the experimental data of both GaAs/AlAs superlattices and Si/Ge superlattices are close to the calculations in Figs. 8(a) and 9(a), a more realistic treatment on the specific heat and phonon group velocity leads to over-prediction of the thermal conductivity based on the elastic-acoustic-mismatch model, as demonstrated by Figs. 8(b) and 9(b). The experimental data can be better explained based on the inelastic acoustic mismatch model, as can be seen from Figs. 8(d) and 9(d). These calculations lead to an interface specularity parameter ~ 0.8 , a value close to the one obtained

in modeling the in-plane superlattice thermal conductivity.¹⁵ We should point out that phonon confinement has been experimentally confirmed in many superlattices.¹³ These experiments were done for phonons in specific directions (typically normal incidence), and they did not yield quantitatively how much phonons were actually confined. The above results indicate that in terms of total heat flux, the phonon confinement effect is small. The conclusion that inelastic scattering plays a role in the observed thermal conductivity of superlattices also agrees with lattice-dynamic simulation results by Stoner and Maris³² on the interface TBR.

There are several possible explanations for the mechanisms of the diffuse interface scattering of phonons. The most obvious one is the interface roughness. It is well known that even the best superlattices have certain interface structures such as long-range terraces and short-range mixing of atoms.³⁹ At molecule-beam-epitaxy-grown GaAs/Al_xGa_{1-x}As interfaces, roughness often extends to 1–3 atomic layers, or ~ 3 –9 Å. This roughness is comparable to the dominant phonon wavelength,¹⁵ and will cause diffuse scattering of phonons. The effect of interface roughness on phonon propagation has been reported in direct phonon imaging experiments.⁴⁰ Many studies have been carried out to investigate the effects of interface roughness on the phonon dispersion and Raman spectrum of superlattices.^{41–43} The effect of interface roughness on the TBR of a single interface is also a subject of numerous studies.³¹ In addition to the diffuse scattering caused by interface roughness, two other mechanisms may also cause the diffuselike scattering. These are the inelastic scattering caused by the anharmonic interatomic force interaction and the phonon mode conversion at the interface. Due to the existence of these processes, the phonon distribution at the interface may not follow the simplified model used in this work, i.e., the interface scattering may be neither partially diffuse nor partially specular.

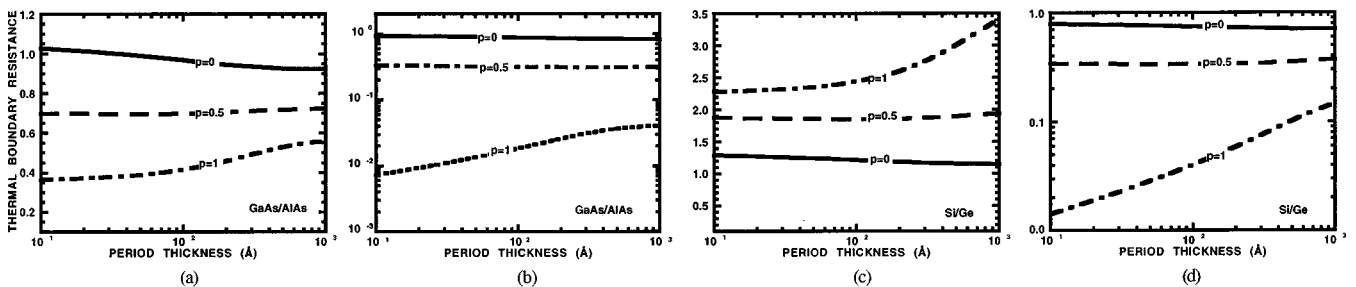


FIG. 7. Normalized thermal boundary resistance as a function of layer thickness for GaAs/AlAs and Si/Ge superlattices under the elastic acoustic mismatch model [(a) and (c)], and under the inelastic acoustic mismatch model [(b) and (d)].

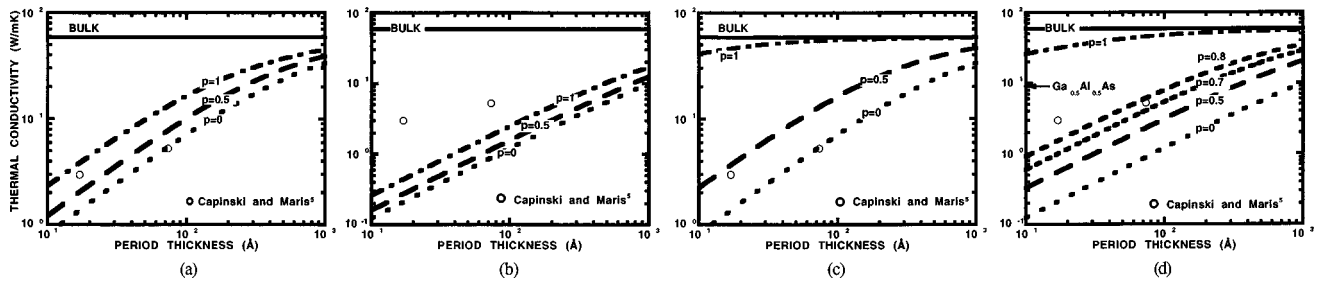


FIG. 8. Thickness dependence of the thermal conductivity of GaAs/AlAs superlattices [(a) and (b)] under the elastic, and [(c) and (d)] under the inelastic acoustic mismatch model. (a) and (c) are based on the the total specific heat and the speed of sound, while (b) and (d) are based on the exclusion of optical phonons and a spectrally averaged phonon group velocity.

Modeling of the more general case that includes the detailed interface scattering processes is beyond of the scope of this work.

For Si/Ge, there is also a sudden reduction in the thermal conductivity with increasing layer thickness. Reference 7 indicated that this reduction is due to the existence of dislocations. Chen and Neagu²³ used a dislocation scattering model, and indeed calculated a comparable reduction of thermal conductivity at a dislocation density $\sim 10^{12}$ cm⁻². At this dislocation density, the dominant scattering mechanism is due to strain field around the dislocations. Because the dislocation scattering is a bulk process, the measured thermal conductivity becomes thickness independent.

Although the elastic acoustic mismatch model has been ruled as an unlikely interface scattering process, it is interesting to note that in this case, the thermal conductivity of GaAs/AlAs superlattices depends on the interface specularity parameter differently from that of Si/Ge superlattices, as shown in Figs. 8(a) and 9(a). For GaAs/AlAs superlattices, increasing the interface specularity parameter increases the thermal conductivity, while, for Si/Ge superlattices, the thermal conductivity decreases with the increasing interface specularity parameter. This is because of the large acoustic mismatch between Si and Ge compared to that between GaAs and AlAs. The average reflectivity at a Si/Ge interface calculated based on the elastic acoustic mismatch model is larger than that based on the diffuse scattering model, thus increasing the interface specularity parameter increases the TBR, while the reverse is true for a GaAs/AlAs interface. The overall differences in the reflectivity between the diffuse mismatch and elastic acoustic mismatch models are small, and thus the spread of the thermal conductivity under the two models is small. Under the inelastic acoustic mismatch model, the specular reflectivity is relatively weak for both

Si/Ge and GaAs/AlAs superlattices and the thermal conductivity becomes sensitive to the interface specularity parameter around the totally specular scattering interface limit, similar to the in-plane thermal conductivity.¹⁵ The sensitivity of the cross-plane thermal conductivity to the interface specularity parameter is shown in Figs. 10(a) and 10(b) for the two different models on the specular interfaces, i.e., the elastic and the inelastic acoustic mismatch models.

Figures 11(a) and 11(b) compare the calculated temperature dependence of the thermal conductivity of Si/Ge and GaAs/AlAs superlattices with experimental data of Refs. 7 and 5. Only results obtained from the consideration of the phonon dispersion and the inelastic scattering at the boundary are presented. For Si/Ge superlattices, the model results are in reasonable agreement with the experimental data. For GaAs superlattices, the model is able to explain the experimental data on the 12×14 superlattice (12 ML of GaAs and 14 ML of AlAs). For the 3×3 superlattice, the model predicts the correct order of magnitude in the thermal conductivity reduction, but cannot explain well the temperature dependence. Two mechanisms may be responsible for the stronger measured temperature dependence of the thermal conductivity of this superlattice. One of the mechanism is the phonon wave effect such as tunneling and interference, in analogy to the photon tunneling and interference through a narrow gap.^{44,45} Our modeling on the heat conduction through a Ge/Si/Ge double heterojunction structure indicates that tunneling can increase the thermal conductivity of a 10-Å layer by 20%,²⁹ but tunneling alone cannot explain the observed stronger-than-predicted temperature dependence of the thermal conductivity of the 3×3 superlattice. The stronger temperature dependence of the thermal conductivity of this superlattice can be explained by assuming that the specularity parameter is a function of temperature. Although

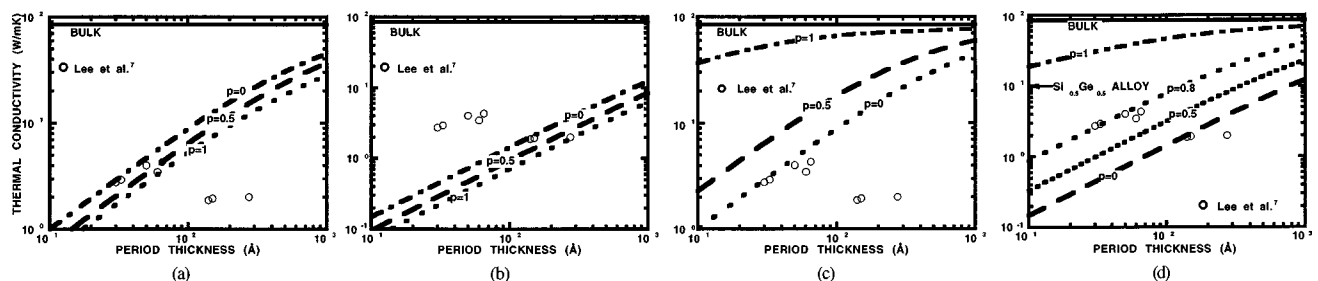


FIG. 9. Thickness dependence of the thermal conductivity of Si/Ge superlattices [(a) and (b)] under the elastic model, and [(c) and (d)] under the inelastic acoustic mismatch model. (a) and (c) are based on the the total specific heat and the speed of sound, while (b) and (d) are based on the exclusion of optical phonons and a spectrally averaged phonon group velocity.

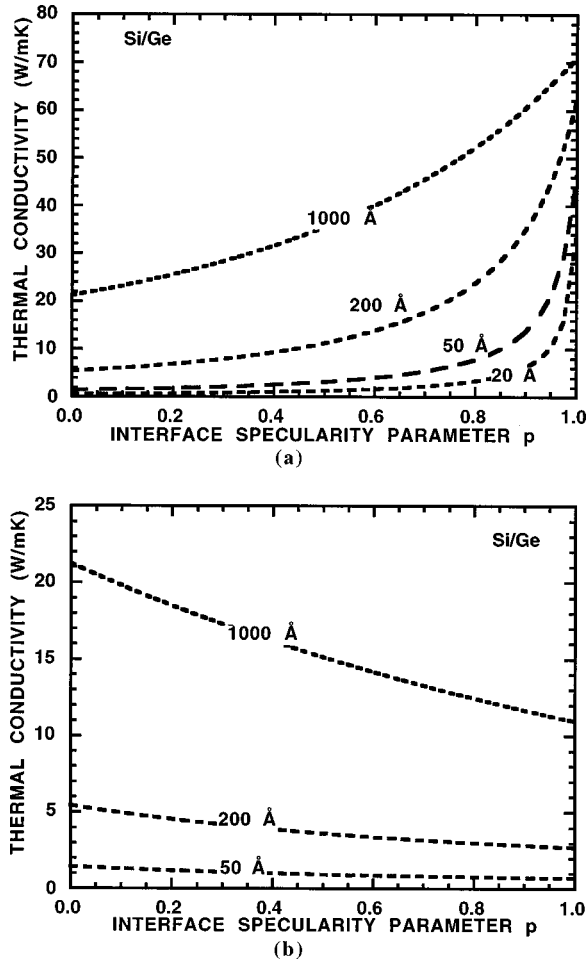


FIG. 10. Sensitivity of thermal conductivity to the interface specularity parameter for Si/Ge superlattices: (a) inelastic acoustic mismatch model and (b) elastic acoustic mismatch model.

the variation of p with temperature is small, its effect on very thin films is strong, as indicated in Fig. 10(a).

The approximate expressions, Eqs. (46), (48), and (49) can be expected to be valid for the cases where the majority of temperature drop in superlattices occurs at interfaces. This is the case for totally diffuse interfaces with very thin superlattice period. Similar is true for specular interfaces with phonon confinement. For specular interfaces under the inelastic-acoustic-mismatch model, the approximate expressions are no longer valid because the interface TBR is very small. Figure 5(c) shows, however, that as long as a small fraction of phonons are diffusely scattered, the TBR increases significantly and the approximation expressions become applicable. Figures 12(a) and 12(b) support the above discussion by comparing the numerical solutions of the BTE with results obtained from the approximate expressions.

The above results and discussion demonstrate that the cross-plane thermal conductivity of superlattices is controlled by the interface scattering of phonons. The temperature drop inside the layers is small compared to the temperature drop at interfaces, i.e., phonon transport across superlattices is ballistic and thermal conductivity is less affected by the scattering mechanisms in bulk materials. For superlattices with layer thickness thinner than the phonon MFP, the effective thermal conductivity is almost exclu-

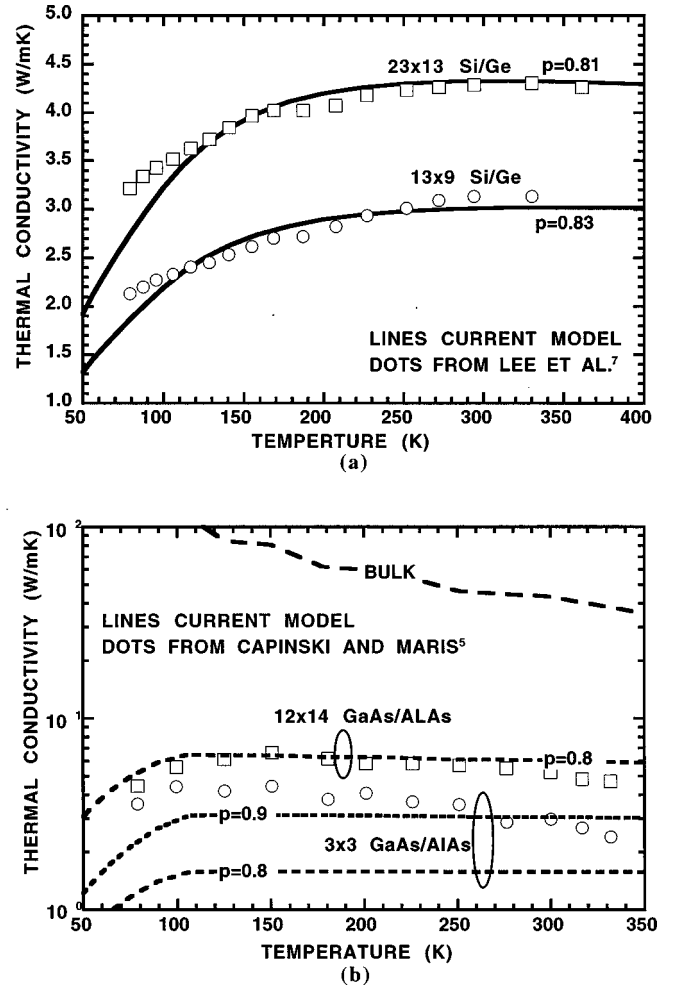


FIG. 11. Temperature dependence of the thermal conductivity of (a) Si/Ge and (b) GaAs/AlAs superlattices.

sively controlled by the interfaces and is independent of the bulk scattering processes. This indicates that many good thermal conductors may be engineered to yield low thermal conductivity structures, and thus opens a way to engineer materials for thermoelectric applications.

It is also interesting to compare the cross-plane thermal conductivity modeling with the in-plane modeling. For the in-plane modeling, the superlattice thermal conductivity always depends on the phonon MFP in bulk materials.^{15,46} Due to this dependence, it becomes necessary to include the frequency dependence of the relaxation time in the in-plane thermal conductivity modeling. For the cross-plane thermal conductivity modeling, since the thermal conductivity at the very thin-film limit is almost totally independent of the bulk relaxation time, we do not expect a large difference in the effective thermal conductivity calculated based on the gray-medium approximation and the frequency-dependence treatment of the phonon MFP.

IV. CONCLUSIONS

Thermal conductivity of superlattices is of current interest for microelectronic and thermoelectric applications. Large reductions on the thermal conductivity of superlattices have been observed in recent years. In this work, we carry out

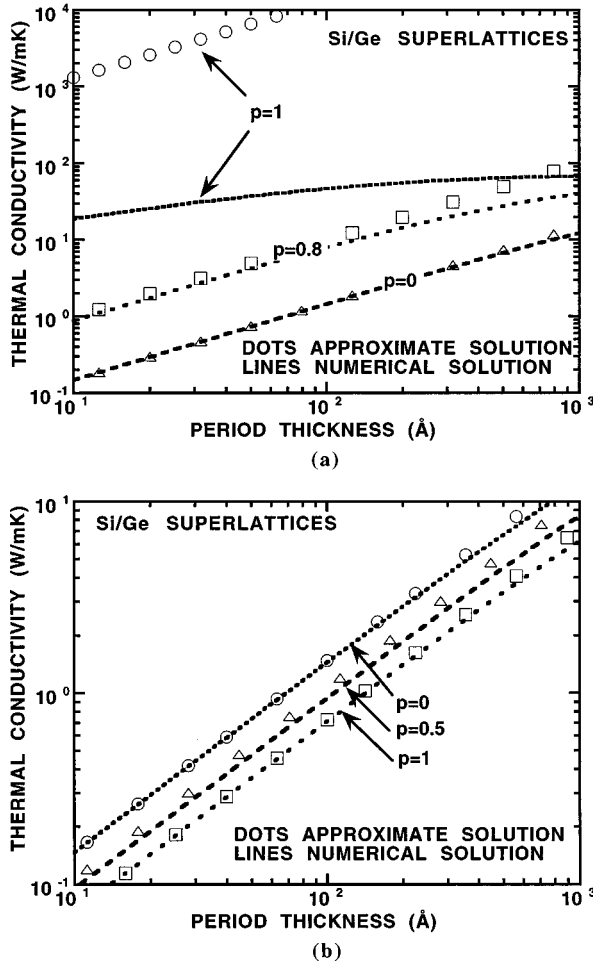


FIG. 12. Comparison of numerical results and approximate solution for (a) the inelastic acoustic mismatch model and (b) the elastic acoustic mismatch model.

theoretical investigations on heat conduction mechanisms in superlattice structures in the direction perpendicular to the film plane based on solving the BTE. Several models for the interface scattering processes are established by extending the acoustic mismatch model and the diffuse mismatch model previously developed in the study of the TBR to include the possibility of phonon confinement and inelastic scattering at interfaces. These models are incorporated into the boundary conditions of the BTE. Computational strategies were developed for numerical solution of the BTE. Approximate analytical solutions are also obtained for the effective cross-plane thermal conductivity of superlattice structures. These analytical solutions are shown to be very good at the thin-film limit.

Results of this study demonstrate that the equivalent thermal conductivity of superlattices is controlled by both the size effects on heat transfer within each layer and the TBR between different layers when the superlattice period thickness is comparable to the phonon MFP. The TBR is no longer an intrinsic property of the interface, but also depends on the layer thickness. When the period thickness is thinner than the phonon MFP in their corresponding bulk materials, the TBR at the interfaces becomes the major factor limiting the thermal conductivity in this direction. Comparison of the modeling results with recent experimental data on Si/Ge and

GaAs/AlAs superlattices suggests that the measured thermal conductivity can be explained by assuming that phonon transport at the interfaces is partially diffuse and partially specular, and that inelastic phonon scattering occurs at the interfaces.

It is clear from this study that the large thermal conductivity reduction experimentally observed in GaAs/AlAs and Si/Ge superlattices results from the interface scattering of phonons. Phonon transport in thin period superlattices is ballistic, and the thermal conductivity of superlattices is almost independent of the scattering mechanisms in bulk materials but is determined by the mismatch of specific heat, group velocity, and density of adjacent layers. Based on this conclusion, we can envision the possibility of engineering superlattices to obtain low thermal conductivity structures even from good bulk thermal conductors. These low thermal conductivity structures may have applications in thermoelectric devices.

Our model cannot explain satisfactorily the experimental thermal conductivity data of a 3×3 GaAs/AlAs superlattice. Possible reasons are due to phonon tunneling and the temperature dependence of the interface specularity parameter. Tunneling increases the heat conduction through superlattices, and the interface specularity parameter may increase with decreasing temperature. These two effects can lead to higher-than-predicted thermal conductivity as well as stronger temperature dependence.

ACKNOWLEDGMENTS

The author would like to thank Professor G. D. Mahan for critically reading the manuscript and gratefully acknowledges financial support by the National Science Foundation Grant No. CTS-9796247 and a DOD MURI program on thermoelectrics.

APPENDIX

In this appendix, we prove that the solution for the deviation of intensity i_i^+ and i_i^- must be antisymmetric. The proof starts from Eq. (5), which can be written as

$$\cos \theta_1 \frac{\partial i_1^+(\theta_1, \eta_1)}{\partial \eta_1} + i_1^+(\theta_1, \eta_1) = -\cos \theta_1 \frac{dI_{01}(\eta_1)}{d\eta_1} \quad (0 < \theta_1 < 90^\circ), \quad (\text{A1})$$

$$\cos \theta_1 \frac{\partial i_1^-(\theta_1, \eta_1)}{\partial \eta_1} + i_1^-(\theta_1, \eta_1) = -\cos \theta_1 \frac{dI_{01}(\eta_1)}{d\eta_1} \quad (90^\circ < \theta_1 < 180^\circ). \quad (\text{A2})$$

Introducing the transformations

$$\varphi_1 = \pi/2 - \theta_1 \quad \text{and} \quad \zeta_1 = \xi_1 - \eta_1, \quad (\text{A3})$$

Equation (A2) becomes

$$\begin{aligned} \cos \varphi_1 \frac{\partial i_1^-(\pi - \varphi_1, \zeta_1)}{\partial \zeta_1} + i_1^-(\pi - \varphi_1, \zeta_1) \\ = \cos \varphi_1 \frac{dI_{01}(\eta_1)}{d\eta_1} \quad (0 < \varphi_1 < 90^\circ). \end{aligned} \quad (\text{A4})$$

The above equation is identical to Eq. (A1) if

$$i_1^+(\theta_1, \eta_1) = -i_1^-(\pi - \theta_1, \zeta_1)$$

or

$$i_1^+(\mu_1, \eta_1) = -i_1^-(\mu_1, \xi_1 - \eta_1). \quad (\text{A5})$$

Such an antisymmetry relation will hold if it can also be proven that the boundary conditions are not violated. Equations (13) and (15) yield

$$\begin{aligned} & i_1^+(0, \mu_1) - p[R_{s12}(\mu_1)i_1^-(0, -\mu_1) + t_{s21}(\mu_2)i_2^+(\xi_2, \mu_2)] \\ & - 2(1-p) \left[R_{d12} \int_0^1 i_1^-(0, -\mu_1)\mu_1 d\mu_1 \right. \\ & \left. + T_{d21} \int_0^1 i_2^+(\xi_2, \mu_2)\mu_2 d\mu_2 \right] \\ & = \Psi_{12} \Pi_1 [pT_{s12}(\mu_1) + pT_{d12}] \end{aligned} \quad (\text{A6})$$

and

$$\begin{aligned} & i_1^-(\xi_1, -\mu_1) - p[R_{s12}(\mu_1)i_1^+(\xi_1, \mu_1) + t_{s21}(\mu_2)i_2^-(0, -\mu_2)] \\ & - 2(1-p) \left[R_{d12} \int_0^1 i_1^+(\xi_1, \mu_1)\mu_1 d\mu_1 \right. \\ & \left. + T_{d21} \int_0^1 i_2^-(0, -\mu_2)\mu_2 d\mu_2 \right] \\ & = \Psi_{21} \Pi_1 [pT_{s12}(\mu_1) + pT_{d12}]. \end{aligned} \quad (\text{A7})$$

If Eq. (A5) and the corresponding equation for i_2 are satisfied, and in addition, if the TBR is symmetric, i.e., $\Psi_{12} = \Psi_{21}$, the above two boundary conditions become identical. Numerical solution shows that the TBR is indeed symmetric. The antisymmetric relations are thus proved.

-
- ¹L. D. Hicks and M. S. Dresselhaus, Phys. Rev. B **47**, 12 727 (1993).
- ²L. D. Hicks, T. C. Harman, X. Sun, and M. S. Dresselhaus, Phys. Rev. B **53**, R10 493 (1996).
- ³G. Chen, C. L. Tien, X. Wu, and J. S. Smith, J. Heat Transfer **116**, 325 (1994).
- ⁴T. Yao, Appl. Phys. Lett. **51**, 1798 (1987).
- ⁵W. S. Capinski and H. J. Maris, Physica B **219**, 699 (1996).
- ⁶X. Y. Yu, G. Chen, A. Verma, and J. S. Smith, Appl. Phys. Lett. **67**, 3554 (1995).
- ⁷S.-M. Lee, D. Cahill, and R. Venkatasubramanian, Appl. Phys. Lett. **70**, 2957 (1997).
- ⁸R. Venkatasubramanian, Nav. Res. News **XLVIII**, 31 (1996).
- ⁹Z. C. Zhang *et al.*, Thin Solid Films **186**, 361 (1990).
- ¹⁰Z. L. Wu, L. H. Wei, and P. K. Kuo, Proc. SPIE **1848**, 361 (1992).
- ¹¹V. Narayanamurti, H. L. Stormer, M. A. Chin, A. C. Gossard, and W. Wiegmann, Phys. Rev. Lett. **43**, 2012 (1979).
- ¹²S. Tamura, D. C. Hurley, and J. P. Wolfe, Phys. Rev. B **38**, 1427 (1989).
- ¹³C. Colvard, T. A. Gant, M. V. Klein, R. Merlin, R. Fisher, H. Morkoc, and A. C. Gossard, Phys. Rev. B **31**, 2080 (1985).
- ¹⁴L. Esaki and R. Tsu, IBM J. Res. Dev. **14**, 61 (1970).
- ¹⁵G. Chen, J. Heat Transfer **119**, 220 (1996).
- ¹⁶C. R. Tellier and A. J. Tossier, *Size Effects in Thin Films* (Elsevier, Amsterdam, 1982).
- ¹⁷C. L. Tien and G. Chen, J. Heat Transfer **116**, 799 (1994).
- ¹⁸S. Y. Ren and J. D. Dow, Phys. Rev. B **25**, 3750 (1982).
- ¹⁹J. Callaway, Phys. Rev. **113**, 1046 (1959).
- ²⁰P. Hyldgaard and G. D. Mahan, *Thermal Conductivity* (Technomic, Lancaster, 1995), Vol. 23, p. 172.
- ²¹G. Chen, in *Micro-Electro-Mechanical-Systems*, Proceedings of the ASME International Mechanical Engineering Congress (ASME, New York, 1996), Vol. DSC-59, p. 13.
- ²²P. Hyldgaard and G. D. Mahan, Phys. Rev. B **56**, 10 754 (1977).
- ²³G. Chen and M. Neagu, Appl. Phys. Lett. **71**, 2761 (1997).
- ²⁴A. Majumdar, J. Heat Transfer **115**, 7 (1993).
- ²⁵G. Chen, J. Heat Transfer **118**, 539 (1996).
- ²⁶R. Siegel and J. Howell, *Thermal Radiation Heat Transfer* (Hemisphere, Washington, 1993).
- ²⁷N. W. Ashcroft and N. D. Mermin, *Solid State Physics* (Saunders, Philadelphia, 1976).
- ²⁸O. Weis, in *Nonequilibrium Phonons in Nonmetallic Crystals*, edited by W. Eisenmenger and A. A. Kaplyanskii (North-Holland, Amsterdam, 1986), p. 1.
- ²⁹G. Chen, *Proceedings of the 7th AIAA/ASME Joint Thermophysics and Heat Transfer Conference* (ASME, New York, 1998), Vol. 3, p. 205.
- ³⁰W. A. Little, Can. J. Phys. **37**, 334 (1959).
- ³¹E. T. Swartz and R. O. Pohl, Rev. Mod. Phys. **61**, 605 (1989).
- ³²R. J. Stoner and H. J. Maris, Phys. Rev. B **48**, 16 373 (1993).
- ³³S. Simons, J. Phys. C **7**, 4048 (1974).
- ³⁴J. A. Katerberg, C. L. Reynolds, Jr., and A. C. Anderson, Phys. Rev. B **16**, 673 (1977).
- ³⁵G. A. Slack, Solid State Phys. **34**, 1 (1979).
- ³⁶G. P. Srivastava, J. Phys. Chem. Solids **41**, 357 (1980).
- ³⁷E. Castano and G. Kirczenow, Phys. Rev. B **41**, 5055 (1990).
- ³⁸S.-Q. Yuan and B.-Y. Gu, J. Appl. Phys. **73**, 7496 (1993).
- ³⁹M. H. Bode and A. Ourmazd, J. Vac. Sci. Technol. B **10**, 1787 (1992).
- ⁴⁰D. C. Hurley, S. Tamura, J. P. Wolfe, and H. Morkoc, Phys. Rev. Lett. **58**, 2446 (1987).
- ⁴¹D. Kechrakos, P. R. Briddon, and J. C. Inkson, Phys. Rev. B **44**, 9114 (1991).
- ⁴²T. Ruf, J. Spitzer, V. F. Sapega, V. I. Belitsky, M. Cardona, and K. Ploog, Phys. Rev. B **50**, 1792 (1994).
- ⁴³B. Jusserand, Phys. Rev. B **42**, 7256 (1990).
- ⁴⁴G. A. Domoto, R. F. Boehm, and C. L. Tien, J. Heat Transfer **92**, 412 (1970).
- ⁴⁵G. Chen, Microscale Thermophys. Eng. **1**, 215 (1997).
- ⁴⁶G. Chen and C. L. Tien, J. Thermophys. Heat Transfer **7**, 311 (1993).